Applied Catalysis B: Environmental 254 (2019) 551–559

Contents lists available at ScienceDirect

Applied Catalysis B: Environmental

journal homepage: www.elsevier.com/locate/apcatb

Sacrificing ionic liquid-assisted anchoring of carbonized polymer dots on perovskite-like $PbBiO_2Br$ for robust CO_2 photoreduction

Bin Wang[a], Jun Di[a], Lei Lu[b], Shicheng Yan[b], Gaopeng Liu[a], Yuzhen Ye[a], Haitao Li[a,c], Wenshuai Zhu[a,*], Huaming Li[a], Jiexiang Xia[a,*]

[a] School of Chemistry and Chemical Engineering, Institute for Energy Research, Jiangsu University, Zhenjiang, 212013, China
[b] Eco-Materials and Renewable Energy Research Center (ERERC), National Laboratory of Solid State Microstructures, College of Engineering and Applied Sciences, Nanjing University, Nanjing, 210093, China
[c] School of Chemical and Biomolecular Engineering, Faculty of Engineering & Information Technologies, The University of Sydney, Sydney, 2006, Australia

ARTICLE INFO

Keywords:
CPDs
$PbBiO_2Br$
Ionic liquid
Composite photocatalysts
CO_2 reduction

ABSTRACT

The semiconductor-mediated solar-driven the conversion of CO_2 into the value-added fuels is considered as an ideal strategy for sustainable development. However, conventional semiconductors usually suffer from unsatisfactory photocatalytic performance due to the low efficiency of photo-induced carrier separation and sluggish interface adsorption/desorption equilibrium of reactants/products. Herein, novel carbonized polymer dots (CPDs)/$PbBiO_2Br$ heterojunction photocatalysts have been prepared via self-sacrificing ionic liquid, which not only act as the template and reactant to induce the formation of $PbBiO_2Br$ material, but also act as the glue to in situ anchor CPDs on the surface of $PbBiO_2Br$ material to form composites through hydrogen bond. Without sacrificial reagent, the obtained CPDs/$PbBiO_2Br$ materials synthesized with ionic liquid exhibit a high selectivity, stability and enhanced CO evolution rate in water. The introduction of CPDs not only effectively promote the light absorbance and separation efficiency of photogenerated electrons, but also adjust the adsorption/desorption equilibria of reactants/products on the CPDs/$PbBiO_2Br$ catalyst surface, such as boosting CO_2 adsorption capacity, proton affinity and CO liberation. The reaction mechanism has been proposed with in situ FT-IR spectrometry. The strategy for the preparation of high-performance CO_2 photoreduction catalysts can be extended to design and tune other advanced photocatalytic materials.

1. Introduction

Producing valuable chemicals from CO_2 as carbon source is considered as one of the most promising strategies for developing renewable alternatives to fossil fuels in the future [1]. Photocatalytic CO_2 reduction has attracted much attention because of utilizing inexhaustible sunlight as energy source and cheap water as a reductant to reduce CO_2 to obtain valuable fuels [2]. However, the activation and transformation of photocatalytic CO_2 is still a challenge on account of the stable chemical properties and high activation energy barriers of CO_2 [3,4]. In addition, semiconductor photocatalysts also contain a series of weakness, such as (1) the semiconductor catalyst (such as TiO_2, ZnO) with wide band gap only absorb UV light, while the UV light is merely 4% of the total solar light spectrum; (2) high photogenerated carrier recombination efficiency; (3) sluggish reactants (CO_2 or proton) adsorption capacity or product desorption ability [5,6]. For this purpose, a series of strategies (including morphology control [7], heteroatom doping [8], defect control [9], semiconductor recombination [10], etc.) have been explored to solve these obstacles. However, many of them can only solve one or two problems, and these obstacles could not be overcome completely. Therefore, exploring an effective strategy to break above mentioned bottlenecks completely to enhance the photocatalytic CO_2 reduction activity for semiconductor photocatalyst, thus the practical application of the photocatalyst is expected.

Recently, bismuth oxyhalides (BiOX, X = Cl, Br, I), important V-VI-VII ternary Sillén family compounds, have drawn extensive interests in photocatalytic energy conversion and environmental remediation [11,12]. They possess unique layered structure that covalent metal oxygen layers [Bi_2O_2] separated by halide layers along the (001) direction [13]. They exhibit good performance in the photocatalytic field of toxic organic pollutants degradation, water splittng, CO_2 conversion, etc. [14–16]. However, some intrinsic insufficient of BiOX limit their further development, such as low light absorption capacity, high recombination rate of photogenerated carriers. Moreover, during the CO_2

* Corresponding authors.
E-mail addresses: zhuws@ujs.edu.cn (W. Zhu), xjx@ujs.edu.cn (J. Xia).

https://doi.org/10.1016/j.apcatb.2019.04.068
Received 29 January 2019; Received in revised form 15 April 2019; Accepted 20 April 2019
Available online 03 May 2019
0926-3373/

conversion process, the CO_2 adsorption, activation and product desorption capacity of BiOX still are unsatisfactory [17,18]. Therefore, a series of strategies have been explored to enhance the photocatalytic performance of BiOX, such as semiconductor compound, morphological regulation, heterologous hybridization, crystal faces control and bismuth-rich strategy [11–13,19]. Recently, a part of Bi in the $[Bi_2O_2]^{2+}$ layer is replaced by other metal elements (A = Ba, Sr, Cd, Ca, Pb, etc) form a covalent bimetallic oxide ion ($[ABiO_2]^+$) layer [20,21]. The $[ABiO_2]^+$ and $[X]^-$ ion layers are alternately arranged to form $ABiO_2X$ materials. The formation of bismuth-based polymetallic oxyhalides can optimize the photocatalytic performance of bismuth oxyhalide under visible light irradiation. Due to the radius of Pb^{2+} is similar to that of Bi^{3+}, compared to original BiOX, the crystal structure of $PbBiO_2X$ do not display greatly change by replacing Bi^{3+} with Pb^{2+} [22–25]. Among them, the new promising layered materials $PbBiO_2Br$ has been attracted much attention for photocatalytic application, such as, photocatalytic organic synthesis and environment remediation, owing to its suitable band gaps, controllable morphology, high stability and good visible light induced photocatalytic activity [26–30]. Although the $PbBiO_2Br$ catalyst has not been used for photocatalytic CO_2 reduction. Nevertheless, the proper conduction band of the $PbBiO_2Br$ enables the photoelectron to have high reducibility, so that the catalyst has great potential in the field of photocatalytic CO_2 reduction.

In recent years, a novel carbon based nanomaterial, 0D carbonized polymer dots (CPDs) with sizes below 10 nm have been widely concerned [31].They exhibit special properties, including nontoxic, good chemical stability, inexpensive and have been successfully utilized in various fields [32–35]. The conjugated π structure of CPDs makes them excellent electron transporters and acceptors [31]. Therefore, CPDs also have been introduced to photocatalytic applications for the modification of photocatalysts, which can widen the light-harvesting properties of photocatalyst and promote the effective separation of photoconductive carrier, thus improve their utilization of solar energy and photocatalytic CO_2 reduction performance [36–38]. Nonetheless, in most reported systems, the key role of CPDs in the enhanced photocatalytic activity of semiconductors has not been studied in detail, and the mechanism of photocatalytic CO_2 conversion has also not been investigated. In addition, how to effectively anchor CPDs on catalyst surface also is the key to improve efficient utilization of CPDs, thus should be further researched.

To accomplish aforementioned challenging issues, the CPDs modified $PbBiO_2Br$ composite photocatalyst has been prepared via self-sacrificing ionic liquid glue, which conducive to in situ anchor more CPDs on the surface of $PbBiO_2Br$ material, due to the existence of hydrogen bond and coulomb force between ionic liquid and CPDs [39]. The constructed CPDs/$PbBiO_2Br$ heterojunction with intimate contact improve transfer and separation of photo-induced charge carriers across heterojunction interface owing to the intense physical and electronic coupling effects. The introduction of CPDs also promote CO_2 adsorption capacity, proton affinity and CO liberation, thus exhibiting extremely enhanced photocatalytic CO_2 reduction activity. This work is expected to provide some insights for the design and preparation of more efficient CO_2 reduction photocatalysts.

2. Experimental details

2.1. Photocatalyst synthesis

All of reagents are analytical grade and are used as received. The CPDs solid was prepared based on the reported literature and then handled by freeze-drying [40]. 5 mmol citric acid and 335 μL ethylenediamine were dissolved into 10 mL deionized water. After being stirred for 30 min, the mixed solution was added into 25 mL Teflon-lined autoclave and subsequently heated at 200 °C for 5 h. After the autoclaves cool down to room temperature, the acquired product was subjected to dialysis for 24 h in order to obtain the CPDs solution. The CPDs solution was further freeze-dried to obtain CPDs solid.

In a typical procedure of pure $PbBiO_2Br$ and CPDs/$PbBiO_2Br$ materials, 1 mmol $Bi(NO_3)_3{\cdot}5H_2O$, 1 mmol $Pb(NO_3)_2$ and x g CPDs were dissolved into 10 mL acetic acid aqueous solution, which defined as solution A. 1 mmol ionic liquid $[C_{16}mim]Br$ was dissolved into 10 mL ethanol to obtain solution B. Then solution B was dropwise added into solution A with stirring continuously. After stirring for 30 min, the mixed solution was poured into 25 mL Teflon-lined autoclave and subsequently heated at 180 °C for 24 h. After autoclave cool to room temperature, the precipitate was collected and washed with ethanol and deionized water for several times. The final products were dried at 60 °C for 12 h. The added contents of CPDs in CPDs/$PbBiO_2Br$ materials were 1, 3, 5, and 8 wt %, respectively. Pure $PbBiO_2Br$ was prepared without adding CPDs.

For comparison, $PbBiO_2Br$-KBr and CPDs/$PbBiO_2Br$-KBr were prepared via similar methods, merely replacing $[C_{16}mim]Br$ by KBr.

2.2. Materials characterization

The powder X-ray diffraction (XRD) pattern is measured on a Shimadzu XRD-6000X-ray diffractometer with monochromatized Cu-Kα radiation (λ = 0.15418 nm). The X-ray photoelectron spectroscopy (XPS) measured on a PHI5300 with a monochromatic Mg Kα source. The Fourier transform spectrophotometer (FT-IR, Nexus 470, Thermo Electron Corporation) is analyzed using the standard KBr disk method. The morphology of the samples is investigated by scanning electron microscope (SEM) (JEOL JSM-7001 F) and transmission electron microscopy (TEM) (JEOL-JEM-2010) equip with an energy dispersive X-ray spectroscope. The specific surface area and particle size of the photocatalysts are obtained via Brunauer-Emmett-Teller (BET) method based on the N_2 adsorption-desorption isotherms (Micromeritics Instrument Corporarion, USA). CO_2 adsorption isotherms measurements for the samples are carried out a CO_2 adsorption apparatus (Micromeritics Instrument Corporarion, USA). The UV–vis spectra is detected by UV–vis spectrometer on an UV-2450 spectrophotometer (Shimadzu Corporation, Japan) with $BaSO_4$ powder as the reference. The photoluminescence spectra analysis (PL) is detected by a Varian Cary Eclipse spectrometer. The in-situ FT-IR spectra were obtained using in-situ diffuse reflectance infrared Fourier transform spectroscopy (Thermo fisher Nicolet iZ10, USA). Zeta potential measurements were conducted with a Brookhaven Instruments Zeta Potential Analyzer. The photocurrent is measured in phosphate buffer solution (0.1 M PBS, pH = 7.0). The electrochemical impedance spectroscopy (EIS) is tested in a 0.1 M KCl solution containing 5 mM $Fe(CN)_6^{3-}/Fe(CN)_6^{4-}$. The photocurrent and EIS testing results are recorded with the CHI 760E electrochemical system. The Mott-Schottky plots is measured in 0.1 M KCl solution, which is recorded with the Zahner Zennium CIMPS system based on an IM6x electrochemical workstation. The fluorescence life time spectra were recorded on a spectrophotometer (FS5, Edinburgh Instruments Ltd.). Decay curves were analyzed at the emission of 468 nm in prepared materials under 360 nm excitation. The decay curves for samples can be fitted based on the following formula: $I(t) = B + \sum_{i=1}^{N}(A_i)\exp\left(-\frac{t}{\tau_i}\right)$, where N is a number of discrete emissive species, B is a baseline correction, Ai and τi are pre-exponential factors. For multi-exponential decays, the average lifetime, $< \tau >$, can be formulated as: $\langle\tau\rangle = \sum_{i=1}^{N} a_i\tau_i$ and $a_i = \frac{A_1}{\sum A_i}$ where ai is the contribution of the decay component.

2.3. Photocatalytic CO_2 reductions activity measurement

Typically, 100 mg of photocatalyst and 100 mL of H_2O are added into a reactor made of quartz glass (Perfect Light Company, Beijing, China). Then, high purity CO_2 was introduced into the reactor. A xenon (Xe) lamp (300 W, PLS-SXE 300C (BF), Perfectlight, China) was used as light source to trigger the photocatalytic reaction. The reaction

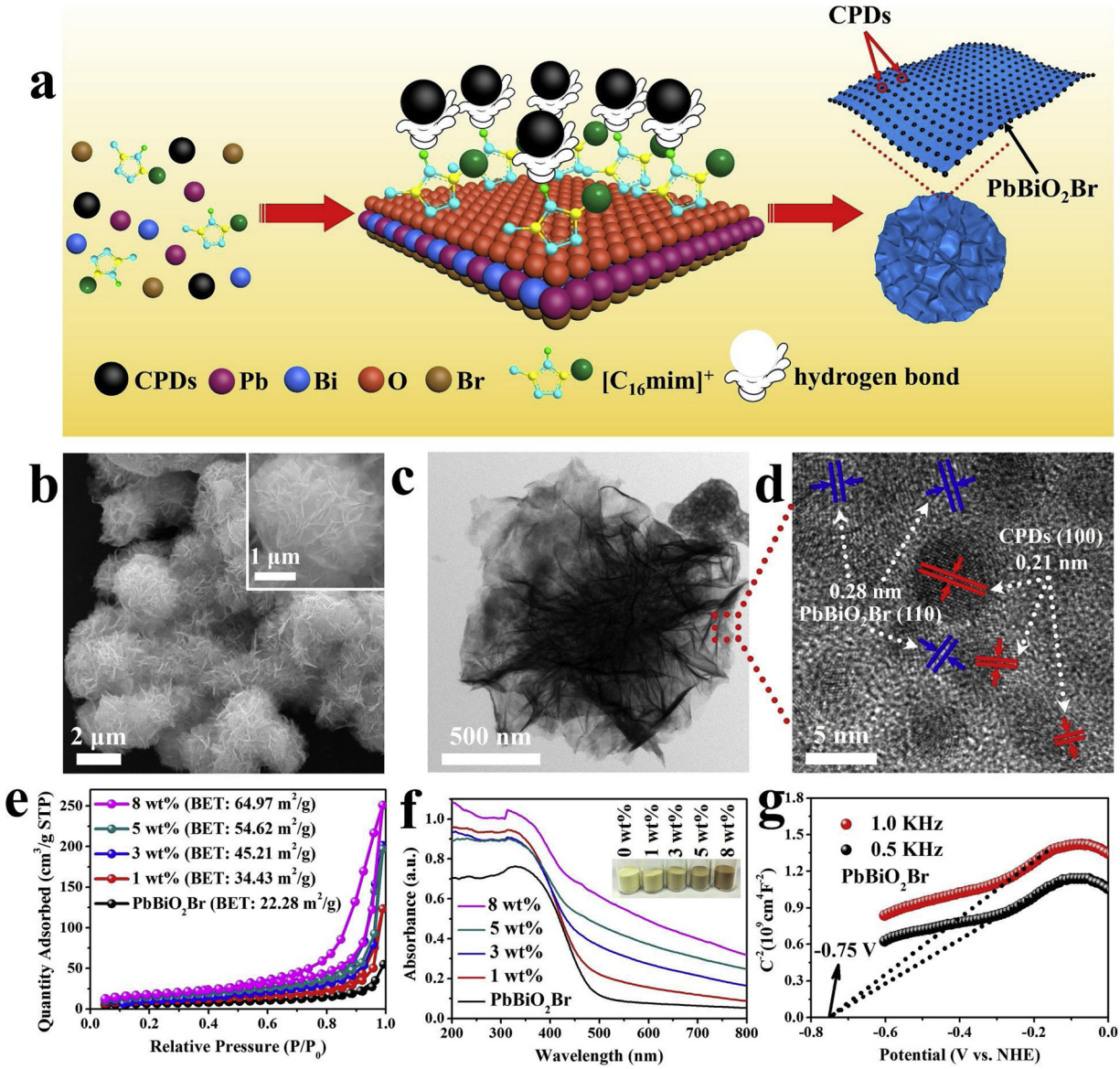

Fig. 1. (a) Illustration for the formation of CPDs/$PbBiO_2Br$ composite material. (b) SEM, (c) TEM and (d) HR-TEM images of 5 wt% CPDs/$PbBiO_2Br$ materials. (e) Nitrogen adsorption-desorption isotherm and (f) UV–vis diffuse reflection spectra of the pure $PbBiO_2Br$ and CPDs/$PbBiO_2Br$ materials. (g) Mott-Schottky plots of the $PbBiO_2Br$.

temperature was kept at 10 °C by a low-temperature thermostat bath system. After each reaction, the gas products were analyzed using a gas chromatography (Shanghai KeChuang Chromatograph Instruments Co., Itd. GC-2002) equipped with a FID detector and a capillary column. The isotope labeling was carried out using $^{13}CO_2$ as carbon source, and ^{13}CO was identified by gas chromatography–mass spectrometry (Agilent 6890 N/5973I, Agilent Corp., USA).

3. Results and discussion

The CPDs material is prepared based on reported literature from citric acid by the hydrothermal process (**Fig. S1**) [40]. The CPDs/$PbBiO_2Br$ composite photocatalysts have been synthesized via self-sacrificing ionic liquid glue [C_{16}mim]Br assisted solvothermal process (Fig. 1a). The 0D CPDs are evenly distributed on the surface of 3D flower like $PbBiO_2Br$ material constructed by ultrathin nanosheets. The XRD analysis indicates all characteristic peaks be assigned to the tetragonal $PbBiO_2Br$ (JCPDS card no. 38-1008) (**Figs. S2a and S3a**). But the typical diffraction peaks of CPDs cannot be found in the XRD pattern. The similar phenomena have also appeared in other previous literatures [41,42]. In FT-IR spectra (**Figs. S2b and S3b**), the absorption bands at 1462 cm^{-1}, 1532 cm^{-1} and 1575 cm^{-1} are observed at CPDs/$PbBiO_2Br$ samples which belongs to typical stretching modes of −COO-, C=O and N−H, respectively [43]. The FT-IR analysis can signify the existence of CPDs in CPDs/$PbBiO_2Br$ material, which is further shown by corresponding Raman spectra (**Fig. S4**), XPS spectra (**Fig. S5**) and EDS analysis (**Figs. S9b and S11**).

SEM and TEM images of pure $PbBiO_2Br$ exhibit 2D ultrathin nanosheets structure (**Fig. S6**), which are similar with $PbBiO_2Br$-KBr (**Fig. S7a-b**). Afte 0D CPDs are introduced, the CPDs with abundant surface functional groups can act as nucleation sites, which induce assembly of 2D $PbBiO_2Br$ nanosheets to 3D porous flower-like structure (Fig. 1**b–c**) (**Figs. S7c-d, S8 and S10**). From **Figs. S9a** and **S10b**, it can be found that numerous dark dots are dispersed on nanosheets, which signifies 0D CPDs have been introduced to $PbBiO_2Br$ uniformly. However, the loading amount of the CPDs in 5 wt% CPDs/$PbBiO_2Br$-KBr is obviously less than that of 5 wt% CPDs/$PbBiO_2Br$. The EDS analysis indicate that CPDs content is about 4.9 wt % and 4.0 wt% in 5 wt% CPDs/$PbBiO_2Br$

and 5 wt% CPDs/$PbBiO_2Br$-KBr materials, respectively. This demonstrate that more CPDs can be anchored on $PbBiO_2Br$ surface using ionic liquids as reaction source when the same CPDs are introduced. This is attributable to the hydrogen bonds formed between the hydrogen atoms at the position 2 in imidazolum ring of ionic liquids and act on the surface carboxyl groups of CPDs [44]. In the HRTEM image (Fig. 1**d**), the lattice fringe spacing of 0.21 nm and 0.28 nm are in accordance with the (100) crystal plane of CPDs and the (110) crystallographic planes of $PbBiO_2Br$ crystallites, respectively [45]. These two crystal plane of CPDs and $PbBiO_2Br$ have tight mutual contaction, which prove that CPDs/$PbBiO_2Br$ heterojunction composite photocatalysts have been prepared successfully, and the CPDs and $PbBiO_2Br$ crystallites have constructed excellent combination.

As shown in Figs. 1**e** and **Fig. S12**, the BET specific surface area and porosity size increase gradually with the enhanced amount of CPDs, which can be conducive to adsorb more CO_2 on the surface of the photocatalysts [46]. The result of surface area and pore diameter distribution analysis are consistent with SEM and TEM analysis. The UV–vis diffuse reflection spectra reveal that the absorption onset of CPDs is about 1400 nm (**Fig. S15a**), and the absorption edge of CPDs/$PbBiO_2Br$ is gradually red-shifted with increasing CPDs amount comparison with pure $PbBiO_2Br$ (Fig. 1f). The $(\alpha E_{photon})^{1/2}$ vs E_{photon} curves of pure $PbBiO_2Br$ and CPDs sample calculated by the classical Tauc approach (**Figs. S13 and S15b**). The band gap energy (E_g) of the $PbBiO_2Br$ and CPDs materials are determined to be nearly 2.17 and 0.67 eV, respectively. The total density of states of valence band (VB) can be determined in valence-band XPS spectra with the Fermi level (E_f) of semiconductors is 0 eV (**Figs. S14** and **S15c**). The VB of CPDs is about 0.64 eV. The VB of both pure $PbBiO_2Br$ and 5 wt% CPDs/$PbBiO_2Br$ are 1.62 eV, which indicate the electronic density of states of $PbBiO_2Br$ cannot be affected after CPDs modified $PbBiO_2Br$ materials.

The positive slopes of Mott-Schotty plots demonstrate both $PbBiO_2Br$ and CPDs are n-type semiconductor characteristics (Figs. 1**g** and **S15d**). According to the extrapolation of X intercept in the Mott-Schotty curves, the flat band potential of $PbBiO_2Br$ and CPDs are ca. -0.75 and -1.20 V vs NHE (pH = 7), respectively. As for the n-type semiconductors, the Fermi level is close to flat band potential [47]. Therefore, the VB of $PbBiO_2Br$ and CPDs are 0.87 and -0.56 V vs NHE, respectively. Based on the formula $E_{CB} = E_{VB} - E_g$, the CB minimum of $PbBiO_2Br$ and CPDs materials occur at about -1.30 and -1.23 V vs NHE, respectively, which confirms the suitable redox potentials of $PbBiO_2Br$ and CPDs to drive CO_2 reduction reaction [48].

The CO_2 photoreduction experiments are carried out in water without sacrificial reagent in the temperature about 10 °C under a 300 W Xe lamp, and predominant reaction product analyzed by gas chromatography is CO. As shown in Fig. 2**a**, pure $PbBiO_2Br$ exhibits the weakest CO yield, and the performance of x wt% CPDs/$PbBiO_2Br$ (x = 1–5) for CO_2 reduction increase first, then decrease along with loading content of 8 wt% CPDs, which is similar with other photocatalytic systems [37,38]. This indicates that the introduction of excess CPDs will inhibit photocatalytic activity of the $PbBiO_2Br$ catalyst. After six hours of illumination, the CO production rates of 5 wt% CPDs/$PbBiO_2Br$ (8.28 μmol h^{-1} g^{-1}) hybrid is 6.68-fold enhancement compared to original $PbBiO_2Br$ (1.24 μmol h^{-1} g^{-1}) (Fig. 2**b**). Meanwhile, the CO evolution rate of 5 wt% CPDs/$PbBiO_2Br$-KBr is greatly lower than that of 5 wt% CPDs/$PbBiO_2Br$ (**Fig. S16**). The effective bonding ability between CPDs and $PbBiO_2Br$ lead to the 5 wt% CPDs/$PbBiO_2Br$ shows the strongest visible light absorbability (**Fig. S17a**), the lowest PL intensity (**Fig. S17b**), the highest photocurrent strength (**Fig. S17c**) and the minimum impedance value (**Fig. S17d**). All these test results certify that the separation efficiency of photogenerated carriers of 5 wt % CPDs/$PbBiO_2Br$ is higher than that of 5 wt% CPDs/$PbBiO_2Br$-KBr. The introduction of self-sacrificing ionic liquid glue plays an important role in this system. Moreover, compared with the WO_3-based, TiO_2-based, ZnO-based and other Bi-based photocatalysts, the CPDs/$PbBiO_2Br$ sample exhibit good photocatalytic CO_2 conversion performance (**Table S1**).

Control experiments demonstrate that the CO_2 photoreduction performance of the physical mixture ($PbBiO_2Br$ and 5 wt% CPDs) is lower than that of 5 wt% CPDs/$PbBiO_2Br$ composite photocatalyst (Fig. 2**c**, column 2), which indicate that the importance of intimate interfacial contact and strong interactions in the heterostructures between CPDs and $PbBiO_2Br$ for the catalytic reaction [49]. During the CO_2 reduction reaction process, if no light irradiation or photocatalyst are provided, there will be no CO generation (Fig. 2**c**, column 3 and 4), which suggest the specific photocatalytic reaction nature [10]. In addition, no obvious CO_2-to-CO conversion reaction is detected without CO_2 or using Ar as the reaction gas, indicating that CO product originates from splitting of CO_2 molecules (Fig. 2**c**, column 5 and 6) [50]. Moreover, the ^{13}C isotope labelling experiment is performed over 5 wt % CPDs/$PbBiO_2Br$ material using $^{13}CO_2$ as substrate to explore carbon source of the evolved CO. As shown in Fig. 2**d**, the peak at $m/z = 29$ in the mass spectra can be assigned to ^{13}CO, which provides strong evidence that the produced CO originates from the photocatalytic reduction of CO_2 molecules. In the Fig. 2**e**, the wavelength-dependent CO_2 photoreduction reactions for 5 wt% CPDs/$PbBiO_2Br$ has been explored, revealing the trend of CO evolution corresponds well with the optical absorption spectrum of the CPDs/$PbBiO_2Br$ material [49,51]. It can indicate the excellent CO_2 photoreduction performance actually induced by the light excitation CPDs/$PbBiO_2Br$ composite photocatalyst. The stability of 5 wt% CPDs/$PbBiO_2Br$ composite material has been investigated by four consecutive runs with each run of 4 h under irradiation (Fig. 2**f**). It can been found that the 5 wt% CPDs/$PbBiO_2Br$ hybrid exhibits good stabilization and light resistance with the potential for long-term photocatalytic applications. **Fig. S18** show the characterization of 5 wt% CPDs/$PbBiO_2Br$ materials after stability testing. After four consecutive runs, the color of catalyst did not change significantly from the digital photographs (**Fig. S18a**). Meanwhile, the invariable XRD patterns of the 5 wt% CPDs/$PbBiO_2Br$ materials before and after the cycling photocatalytic experiments could further confirm the stability of composite photocatalysts (**Fig. S18b**). In **Fig. S18c-d**, the 5 wt% CPDs/$PbBiO_2Br$ maintains its original microscopic morphology with a porous sphere-like structure after CO_2 photoreduction stability test. All these tests can effectively demonstrate that the 5 wt% CPDs/$PbBiO_2Br$ catalyst possesses superior durability.

To clarify the role of CPDs on enhancing CO_2 photoreduction efficiency of CPDs/$PbBiO_2Br$ heterojunction photocatalyst, the photoluminescence and photoelectrochemical characterizations are further conducted. As shown in Fig. 3**a**, the decay curves could be fitted well with a tri-exponential function and the calculated average lifetime values were 5.4 ns for $PbBiO_2Br$ and 8.1 ns for 5 wt% CPDs/$PbBiO_2Br$ composite. Compared with pure $PbBiO_2Br$, CPDs/$PbBiO_2Br$ photocatalyst exhibits increased the radiative lifetime of the charge carriers, which is attributable to the effective transfer of photoelectrons from the conduction band of $PbBiO_2Br$ to CPDs [52]. Furthermore, the steady-state photoluminescence (PL) spectra clarifies that the PL intensity of the CPDs modified $PbBiO_2Br$ hybrid materials decreased to a lower level than that of the pristine $PbBiO_2Br$ (**Fig. S19**). The CPDs with conjugated π structure loaded on the surface of $PbBiO_2Br$ nanosheet can provide an additional energy-transfer pathway in addition to the intrinsic radiative channel for excited-state electron transfer, thus effectively transfer electrons and inhibit the recombination of the photogenerated charge carriers [39]. The electrochemical impedance spectroscopy (EIS) is further carried out to insight the charge-transport behaviors of these two samples, and the result is shown in Fig. 3**b**. The diameter of Nyquist semicircle arc of 5 wt% CPDs/$PbBiO_2Br$/ITO electrode reveals is smaller than that of $PbBiO_2Br$/ITO electrode at high frequencies, suggesting a lower charge-transfer resistance in the CPDs/$PbBiO_2Br$ composite catalyst that permits fast transport and separation of photoinduced charges [53]. Meanwhile, the transient photocurrent spectra with repeatable upon cycling light on and off demonstrates that CPDs/$PbBiO_2Br$ exhibits a higher photocurrent response compared with

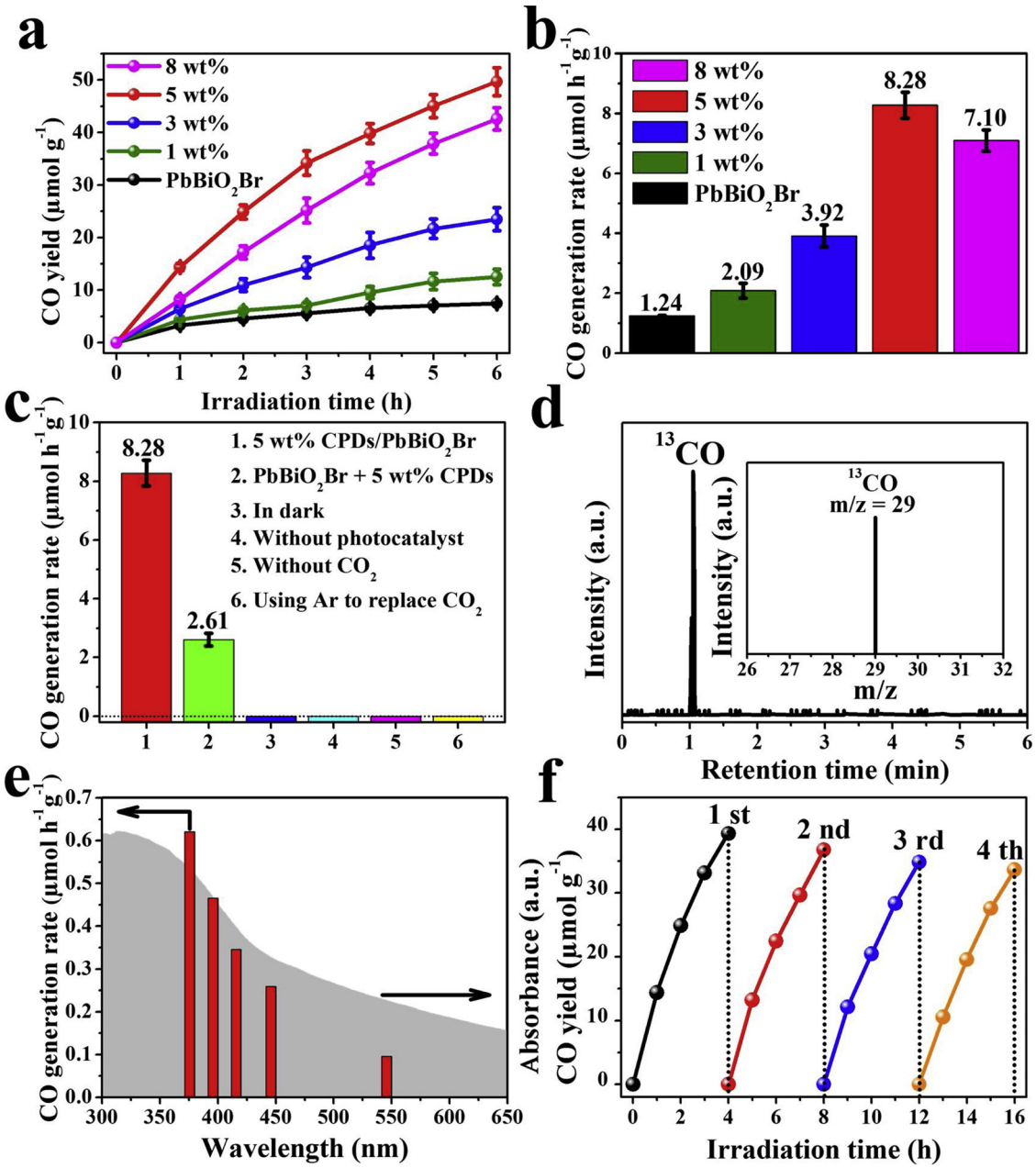

Fig. 2. (a) Time courses of photocatalytic CO evolutions. (b) The CO production rates for six hours under light irradiation. (c) CO_2 reduction performance of the 5 wt % CPDs/$PbBiO_2Br$ under various conditions. (d) mass spectra of ^{13}CO (m/z = 29) produced over 5 wt% CPDs/$PbBiO_2Br$ materials. (e) CO production of the 5 wt% CPDs/$PbBiO_2Br$ under light irradiation with different wavelengths. (f) Cycling runs for the CO_2 photoreduction in the presence of 5 wt% CPDs/$PbBiO_2Br$ materials.

the pure $PbBiO_2Br$ (Fig. 3**c**), which manifests the promoted generation and transfer of photogenerated electron-hole pairs in CPDs/$PbBiO_2Br$ photocatalyst [54]. All these PL and photoelectrochemical characterizations demonstrate that CPDs/$PbBiO_2Br$ photocatalyst can effectively promote generation, transport, and separation of photoinduced charges through the unique CPDs/$PbBiO_2Br$ heterojunction photocatalyst, thereby rendering the higher efficiency of CO_2 photoreduction performance. Moreover, during the CO_2 photoreduction process, the CO_2 adsorption capacity is also generally regarded as another prerequisite [55]. As shown in Fig. 3**d**, 5 wt% CPDs/$PbBiO_2Br$ hybrid photocatalyst exhibit a maximum CO_2 uptake of ~1.28 $cm^3\ g^{-1}$ at 10 °C under 1 atm, much higher than that of original $PbBiO_2Br$ material (~0.62 $cm^3\ g^{-1}$), which indicate CPDs/$PbBiO_2Br$ composite possosses a pronounced advantage in CO_2 adsorption/concentration and suggests its great potential for CO_2 conversion catalysis. Furthermore, the zeta potential value of 5 wt% CPDs/$PbBiO_2Br$ is measured to be -4.92 mV when dispersed in deionized water as compared to that of 9.59 mV for pristine $PbBiO_2Br$ (**Fig. S20**). Because the electronegativity of oxygen is stronger than that of carbon, the carbon is partially positively charged. Therefore, the CPDs/$PbBiO_2Br$ with negative charged surface is conducive to binding carbon element in CO_2 molecules. In addition, it is widely accepted that water can be used as the proton source during the CO_2 photoreduction reaction, thus the close contact between photocatalyst and water will be beneficial to the CO_2 photoreduction activity. For this purpose, the static water contact-angle measurements have been examined (Fig. 3**e**), which display that 5 wt% CPDs/$PbBiO_2Br$ presents a smaller contact angle of 110.8° than that of the pure $PbBiO_2Br$ sample with a contact angle of 125.7°. The smaller water contact angle demonstrates a higher surface hydrophilicity in favour of the surface electron more efficiently transfer to participate the following CO_2 photoreduction reactions [56,57]. Moreover, the CO is the final product of the CO_2 photocatalytic reduction reaction, thus the CO desorption capacity also is a key factor

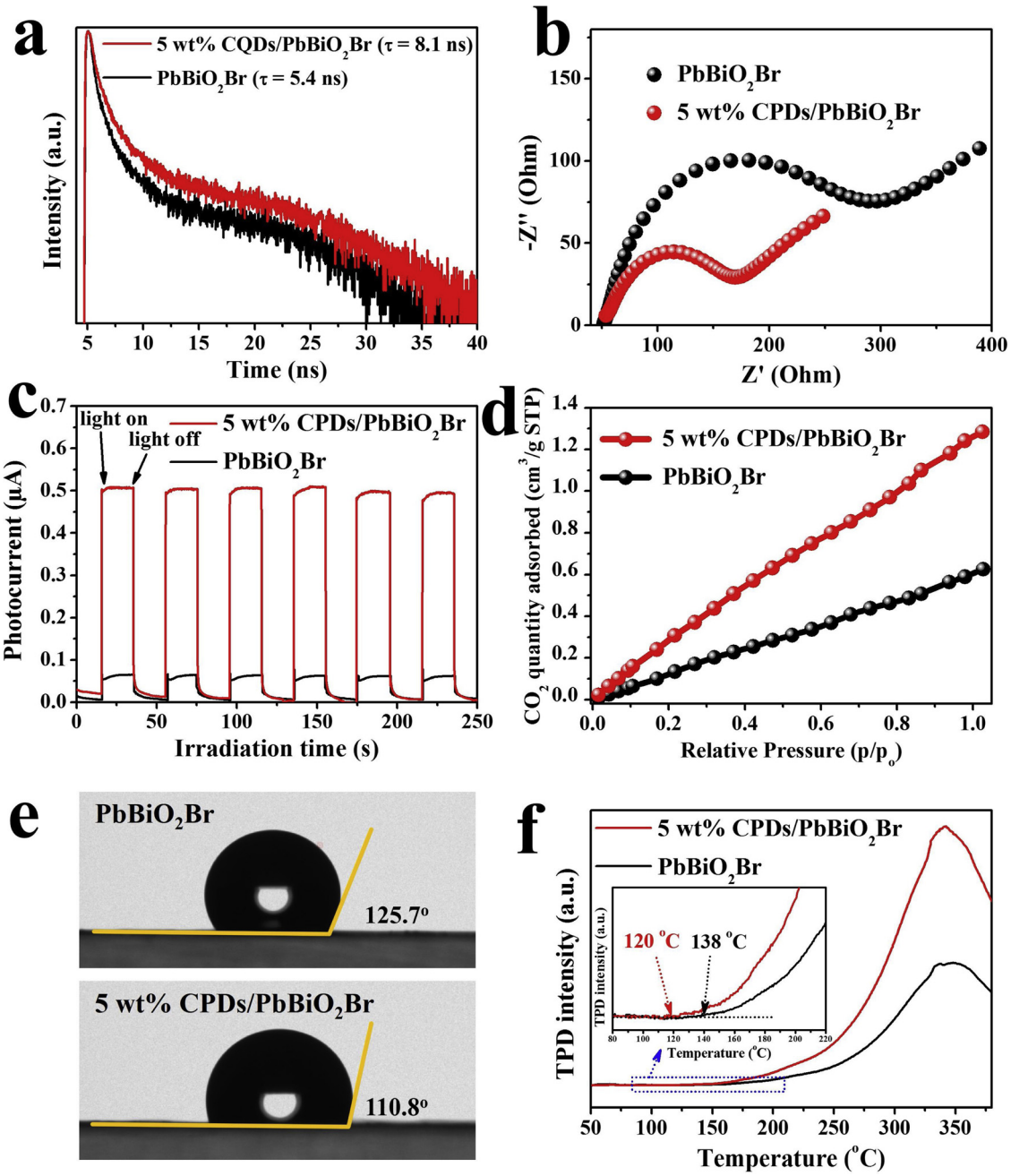

Fig. 3. (a) Time-resolved transient PL decay curve, (b) EIS spectra, (c) transient photocurrent spectra, (d) CO_2 adsorption isotherms, (e) static water contact-angle measurements, (f) CO TPD spectra of $PbBiO_2Br$ and 5 wt% $CPDs/PbBiO_2Br$.

to influence the whole CO_2 reduction processes. From the CO temperature-programmed desorption (TPD) measurements can be found that the lower CO onset desorption temperature and the higher amount of detected CO for the 5 wt% $CPDs/PbBiO_2Br$ indicate the formed CO* molecules can desorb from the surface more easily than that of the pure $PbBiO_2Br$ (Fig. 3**f**) [58]. Consequently, all the above results powerfully illustrated that the CPDs modified $PbBiO_2Br$ heterostructure hybrid photocatalyst completely optimize the vital processes in CO_2 photoreduction reaction, including enhanced photoabsorption, separation and transport of photon-generated carriers, CO_2 adsorption, proton affinity and CO desorption, thus leading to the greatly promoted CO_2 photoreduction performances.

In order to further investigate the CO_2 photoreduction process of the $CPDs/PbBiO_2Br$, in situ Fourier-transform infrared spectroscopy (FT-IR) measurement is performed to gain an in-depth understanding (Fig. 4**a**). To clean the adsorbents on catalyst surface, 5 wt% $CPDs/PbBiO_2Br$ material is first treated at 120 °C under helium atmosphere. After temperature drops to room temperature, CO_2 and H_2O vapor are introduced into the dark environment. When the adsorption desorption equilibrium is maintained, the background can be measured. Subsequently, the FT-IR spectrum will be collected at different light irradiation time. There are a series of IR peaks emerge with increasing irradiation time from 0 to 120 min. The absorption peaks at 1275 and 1583 cm^{-1} are assigned to the bidentate carbonate ($b-CO_3^{2-}$), at 1319, 1473, 1507 and 1542 cm^{-1} are attributable to monodentate carbonate groups ($m-CO_3^{2-}$), at 1418, 1437 and 1456 cm^{-1} are belong to the bicarbonate (HCO_3-), and at 1340, 1525, 1552 and 1716 cm^{-1} are ascribed to the COO- species [59–61]. Among these species, the formation of COOH* as an important intermediate is the rate-limiting step during the photocatalytic conversion of CO_2 to CO [58,62]. The possible

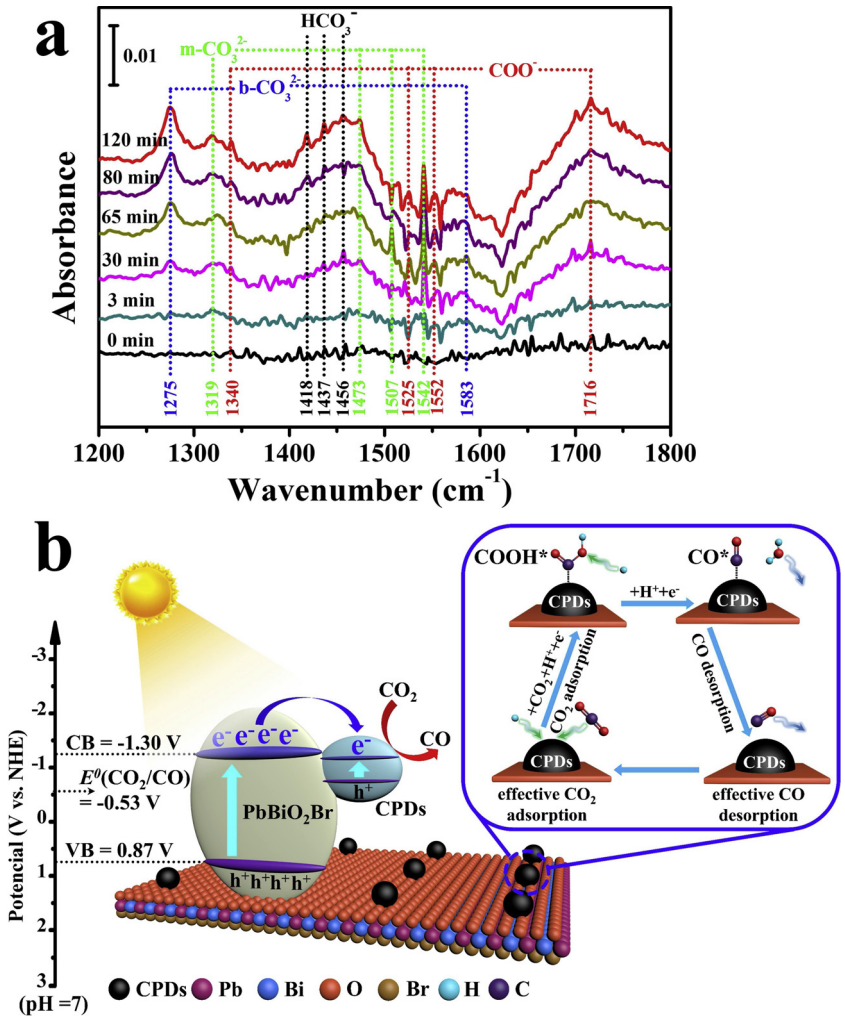

Fig. 4. (a) In situ FTIR spectra for the simulated solar-driven CO_2 reduction process on the 5 wt% CPDs/$PbBiO_2Br$. (b) Schematic of the separation and transfer of photogenerated charges in the CPDs/$PbBiO_2Br$ heterogeneous photocatalyst during CO_2 photoreduction process.

reaction mechanism of solar CO_2 reduction for CPDs/$PbBiO_2Br$ material can be proposed as follows:

$$CO_2\ (g) \rightarrow CO_2^* \quad (1)$$

$$CO_2^* + e^- + H^+ \rightarrow COOH^* \quad (2)$$

$$COOH^* + e^- + H^+ \rightarrow CO^* + H_2O \quad (3)$$

$$CO^* \rightarrow CO \quad (4)$$

where "*" represents the corresponding adsorption state on the catalyst surface.

Based on the above results, the CO_2 photoreduction reaction process diagram of CPDs/$PbBiO_2Br$ photocatalyst is proposed in Fig. 4**b**. Under the light irradiation, the electrons in VB of both $PbBiO_2Br$ and CPDs can be excited to their CB, then form the photogenerated electron-hole pairs. Compared with the CB of $PbBiO_2Br$ (E_{CB} = -1.30 V), the CB of CPDs is slightly smaller than that of $PbBiO_2Br$. Therefore, the photoelectrons of $PbBiO_2Br$ can transfer to the CB of CPDs, which contributes to the effective separation of photoinducded electron-hole pairs. The electron on CPDs will take part in the further process of CO_2 transformation to CO. The adsorbed CO_2* molecules interact with the surface protons will generate the COOH* intermediate gradually, which can transform into CO via the further protonation process. In this photocatalytic system, the introduced CPDs play a crucial role, which act as the electron transfer and photocatalytic reaction centers, thus greatly improved the photocatalytic CO_2 photoreduction activity of CPDs modified $PbBiO_2Br$.

4. Conclusion

In summary, novel CPDs/$PbBiO_2Br$ heterogeneous composite photocatalysts have been synthesized in the presence of self-sacrificing ionic liquid glue via a facile solvothermal method. The introduction of ionic liquids as reaction source is conducive to anchoring more CPDs on the surface of the $PbBiO_2Br$ nanosheets with tight junctions. The CPDs/$PbBiO_2Br$ materials exhibit improved photocatalytic CO_2 reduction activities under ight irradiation, which attributed to enhanced light capture capability, electron transfer and separation ability, CO_2 molecule adsorption, hydrophilia and CO desorption. In situ FTIR spectrometry analysis disclosed that formic acid is a major intermediate. The possible photocatalytic mechanisms have been proposed. This strategy can provide a valuable inspiration to develop other advanced CPDs-based composite photocatalyst materials.

Acknowledgements

This work was financially supported by the National Natural Science Foundation of China (No. 21676128, 21576123, 21476098), and Postgraduate Research & Practice Innovation Program of Jiangsu Province (KYCX17_1792).

Appendix A. Supplementary data

Supplementary material related to this article can be found, in the online version, at doi:https://doi.org/10.1016/j.apcatb.2019.04.068.

References

[1] D. Voiry, H.S. Shin, K.P. Loh, M. Chhowalla, Low-dimensional catalysts for hydrogen evolution and CO2 reduction, Nat. Rev. Chem. 2 (2018) 0105, https://doi.org/10.1038/s41570-017-0105.

[2] L. Zhang, Z.J. Zhao, J.L. Gong, Nanostructured materials for heterogeneous electrocatalytic CO_2 reduction and their related reaction mechanisms, Angew. Chem. Int. Edit. 38 (2017) 11326–11353, https://doi.org/10.1002/anie.201612214.

[3] C.S. Diercks, Y.Z. Liu, K.E. Cordova, O.M. Yaghi, The role of reticular chemistry in the design of CO_2 reduction catalysts, Nat. Mater. 17 (2018) 301–307, https://doi.org/10.1038/s41563-018-0033-5.

[4] X.C. Duan, J.T. Xu, Z.X. Wei, J.M. Ma, S.J. Guo, S.Y. Wang, H.K. Liu, S.X. Dou, Metal-free carbon materials for CO_2 electrochemical reduction, Adv. Mater. 41 (2017) 1701784, , https://doi.org/10.1002/adma.201701784.

[5] X. Liu, S. Inagaki, J.L. Gong, Heterogeneous molecular systems for photocatalytic CO_2 reduction with water oxidation, Angew. Chem. Int. Ed. 55 (2016) 14924–14950, https://doi.org/10.1002/anie.201600395.

[6] N. Elgrishi, M.B. Chambers, X. Wang, M. Fontecave, Molecular polypyridine-based metal complexes as catalysts for the reduction of CO_2, Chem. Soc. Rev. 46 (2017) 761–796, https://doi.org/10.1039/c5cs00391a.

[7] L. Liang, F.C. Lei, S. Gao, Y.F. Sun, X.C. Jiao, J. Wu, S. Qamar, Y. Xie, Single unit cell bismuth tungstate layers realizing robust solar CO_2 reduction to methanol, Angew. Chem. Int. Ed. 54 (2015) 13971–13974, https://doi.org/10.1002/anie.201506966.

[8] I. Shown, S. Samireddi, Y.C. Chang, R. Putikam, P.H. Chang, A. Sabbah, F.Y. Fu, W.F. Chen, C. Wu, T. Yu, P.W. Chung, M.C. Lin, L. Chen, K. Chen, Carbon-doped SnS_2 nanostructure as a high-efficiency solar fuel catalyst under visible ligh, Nat. Commun. 9 (2018) 169, https://doi.org/10.1038/s41467-017-02547-4.

[9] S. Gao, B.C. Gu, X.C. Jiao, Y.F. Sun, X.L. Zu, F. Yang, W.G. Zhu, C.M. Wang, Z.M. Feng, B.J. Ye, Y. Xie, Highly efficient and exceptionally durable CO_2 photoreduction to methanol over freestanding defective single-unit-cell bismuth vanadate layers, J. Am. Chem. Soc. 139 (2017) 3438–3445, https://doi.org/10.1021/jacs.6b11263.

[10] Z.F. Jiang, W.M. Wan, H.M. Li, S.Q. Yuan, H.J. Zhao, P.K. Wong, A hierarchical Z-scheme α-Fe_2O_3/g-C_3N_4 hybrid for enhanced photocatalytic CO_2 reduction, Adv. Mater. 30 (2018) 1706108, , https://doi.org/10.1002/adma.201706108.

[11] L.Q. Ye, Y.R. Su, X.L. Jin, H.Q. Xie, C. Zhang, Recent advances in BiOX (X = Cl, Br and I) photocatalysts: synthesis, modification, facet effects and mechanisms, Environ. Sci. Nano 1 (2014) 90–112, https://doi.org/10.1039/c3en00098b.

[12] H. Li, J. Li, Z.H. Ai, F.L. Jia, L.Z. Zhang, Oxygen vacancy-mediated photocatalysis of BiOCl: reactivity, selectivity, and perspectives, Angew. Chem. Int. Ed. 1 (2018) 122–138, https://doi.org/10.1002/anie.201705628.

[13] J. Di, J.X. Xia, H.M. Li, S.J. Guo, S. Dai, Bismuth oxyhalide layered materials for energy and environmental applications, Nano Energy 41 (2017) 172–192, https://doi.org/10.1016/j.nanoen.2017.09.008.

[14] C.L. Mao, H.G. Cheng, H. Tian, H. Li, W.J. Xiao, H. Xu, J.C. Zhao, L.Z. Zhang, Visible light driven selective oxidation of amines to imines with BiOCl: Does oxygen vacancy concentration matter? Appl. Catal. B: Environ. 228 (2018) 87–96, https://doi.org/10.1016/j.apcatb.2018.01.018.

[15] Y. Yang, C. Zhang, C. Lai, G.M. Zeng, D.L. Huang, M. Zheng, J.J. Wang, F. Chen, C.Y. Zhou, W.P. Xiong, BiOX (X = Cl, Br, I) photocatalytic nanomaterials: Applications for fuels and environmental management, Adv. Colloids Interface 254 (2018) 76–93, https://doi.org/10.1016/j.cis.2018.03.004.

[16] X.L. Jin, L.Q. Ye, H.Q. Xie, G. Chen, Bismuth-rich bismuth oxyhalides for environmental and energy photocatalysis, Coord. Chem. Rev. 349 (2017) 84–101, https://doi.org/10.1016/j.ccr.2017.08.010.

[17] L.Q. Ye, X.L. Jin, C. Liu, C.H. Ding, H.Q. Xie, K.H. Chu, P.K. Wong, Thickness-ultrathin and bismuth-rich strategies for BiOBr to enhance photoreduction of CO_2 into solar fuels, Appl. Catal. B: Environ. 187 (2016) 281–290, https://doi.org/10.1016/j.apcatb.2016.01.044.

[18] M.C. Gao, J.X. Yang, T. Sun, Z.Z. Zhang, D.F. Zhang, H.J. Huang, H.X. Lin, Y. Fang, X.X. Wang, Persian buttercup-like $BiOBr_xCl_{1-x}$ solid solution for photocatalytic overall CO_2 reduction to CO and O_2, Appl. Catal. B: Environ. 243 (2019) 734–740, https://doi.org/10.1016/j.apcatb.2018.11.020.

[19] Z.Y. Ma, P.H. Li, L.Q. Ye, Y. Zhou, F.Y. Su, C.H. Ding, H.Q. Xie, Y. Bai, P.K. Wong, Oxygen vacancies induced exciton dissociation of flexible BiOCl nanosheets for effective photocatalytic CO_2 conversion, J. Mater. Chem. A 5 (2017) 24995–25004, https://doi.org/10.1039/C7TA08766G.

[20] J. Olchowka, H. Kabbour, M. Colmont, M. Adlung, C. Wickleder, O. Mentré, $ABiO_2X$ (A = Cd, Ca, Sr, Ba, Pb; X = halogen) sillen X1 series: polymorphism versus optical properties, Inorg. Chem. 55 (2016) 7582–7592, https://doi.org/10.1021/acs.inorgchem.6b01024.

[21] H. Suzuki, H. Kunioku, M. Higashi, O. Tomita, D. Kato, H. Kageyama, R. Abe, Lead bismuth oxyhalides $PbBiO_2X$ (X = Cl, Br) as visible-light-responsive photocatalysts for water oxidation: role of lone-pair electrons in valence band engineering, Chem. Mater. 30 (2018) 5862–5869, https://doi.org/10.1021/acs.chemmater.8b01385.

[22] A.H. Lee, Y.C. Wang, C.C. Chen, Composite photocatalyst, tetragonal lead bismuth oxyiodide/bismuth oxyiodide/graphitic carbon nitride: Synthesis, characterization, and photocatalytic activity, J. Colloid Interface Sci. 533 (2019) 319–332, https://doi.org/10.1016/j.jcis.2018.08.008.

[23] Y.C. Wang, A.H. Lee, C.C. Chen, Perovskite-like photocatalyst, $PbBiO_2Br$/PbO/g-C_3N_4: Synthesis, characterization, and visible-light-driven photocatalytic activity, J. Taiwan Inst. Chem. Eng. 93 (2018) 315–328, https://doi.org/10.1016/j.jtice.2018.07.037.

[24] F.Y. Liu, J.H. Lin, Y.M. Dai, L.W. Chen, S.T. Huang, T.W. Yeh, J.L. Chang, C.C. Chen, Preparation of perovskites $PbBiO_2I$/PbO exhibiting visible-light photocatalytic activity, Catal. Today 314 (2018) 28–41, https://doi.org/10.1016/j.cattod.2018.02.006.

[25] F.Y. Liu, Y.R. Jiang, C.C. Chen, W.W. Lee, Novel synthesis of $PbBiO_2Cl$/BiOCl nanocomposite with enhanced visible-driven-light photocatalytic activity, Catal. Today 300 (2018) 112–123, https://doi.org/10.1016/j.cattod.2017.04.030.

[26] M. Cherevatskaya, M. Neumann, S. Fuldner, C. Harlander, S. Kummel, S. Dankesreiter, A. Pfitzner, K. Zeitler, B. Konig, Visible-light-promoted stereoselective alkylation by combining heterogeneous photocatalysis with organocatalysis, Angew. Chem. Int. Ed. 51 (2012) 4062–4066, https://doi.org/10.1002/chin.201237040.

[27] X.J. Li, J. Wang, D.Y. Xu, Z. Sun, Q.S. Zhao, W.C. Peng, Y. Li, G.L. Zhang, F.B. Zhang, X.B. Fan, $NbSe_2$ Nanosheet supported $PbBiO_2Br$ as a high performance photocatalyst for the visible light-driven asymmetric alkylation of aldehyde, ACS Sustain. Chem. Eng. 3 (2015) 1017–1022, https://doi.org/10.1021/acssuschemeng.5b00182.

[28] H. Lin, W.W. Lee, S. Huang, L. Chen, T. Yeh, J. Fu, C. Chen, Controlled hydrothermal synthesis of $PbBiO_2Br$/BiOBr heterojunctionwith enhanced visible-driven-light photocatalytic activities, J. Mol. Catal. A 417 (2016) 168–183, https://doi.org/10.1016/j.molcata.2016.03.021.

[29] F.Y. Xiao, J. Xing, L. Wu, Z.P. Chen, X.L. Wang, H.G. Yang, Assembly of ultrathin $PbBiO_2Br$ nanosheets with enhanced visible light photocatalytic properties, RSC Adv. 3 (2013) 10687–10690, https://doi.org/10.1039/c3ra41324a.

[30] B. Wang, J. Di, P.F. Zhang, J.X. Xia, S. Dai, H.M. Li, Ionic liquid-induced strategy for porous perovskite-like $PbBiO_2Br$ photocatalysts with enhanced photocatalytic activity and mechanism insight, Appl. Catal. B 206 (2017) 127–135, https://doi.org/10.1039/C3RA41324A.

[31] S.Y. Lim, W. Shen, Z.Q. Gao, Carbon quantum dots and their applications, Chem. Soc. Rev. 44 (2015) 362–381, https://doi.org/10.1039/C4CS00269E.

[32] M. Han, S.J. Zhu, S.Y. Lu, Y.B. Song, T.L. Feng, S.Y. Tao, J.J. Liu, B. Yang, Recent progress on the photocatalysis of carbon dots: Classification, mechanism and applications, Nano Today 19 (2018) 201–218, https://doi.org/10.1016/j.nantod.2018.02.008.

[33] S.Y. Tao, S.Y. Lu, Y.J. Geng, S.J. Zhu, S.A.T. Redfern, Y.B. Song, T.L. Feng, W.Q. Xu, B. Yang, Design of metal-free polymer carbon dots: a new class of room-temperature phosphorescent materials, Angew. Chem. Int. Ed. 57 (2018) 2393–2398, https://doi.org/10.1002/anie.201712662.

[34] S.Y. Lu, G.J. Xiao, L.Z. Sui, T.L. Feng, X. Yong, S.J. Zhu, B.J. Li, Z.Y. Liu, B. Zou, Mi.X. Jin, J.S. Tse, H. Yan, Bai Yang, Piezochromic carbon dots with two-photon fluorescence, Angew. Chem. Int. Ed. 56 (2017) 6187–6191, https://doi.org/10.1002/anie.201700757.

[35] S.L. Diao, X.J. Zhang, Z.B. Shao, K. Ding, J.S. Jie, X.H. Zhang, 12.35% efficient graphene quantum dots/silicon heterojunction solar cells using graphene transparent electrode, Nano Energy 31 (2017) 359–366, https://doi.org/10.1016/j.nanoen.2016.11.051.

[36] M. Han, S.J. Zhu, S.Y. Lu, Y.B. Song, T.L. Feng, S.Y. Tao, J.J. Liu, B. Yang, Recent progress on the photocatalysis of carbon dots: classification, mechanism and applications, Nano Today 19 (2018) 201–218, https://doi.org/10.1016/j.nantod.2018.02.008.

[37] M.L. Li, M. Wang, L.F. Zhu, Y.M. Li, Z. Yan, Z.Q. Shen, X.B. Cao, Facile microwave assisted synthesis of N-rich carbon quantum dots/dual-phase TiO_2 heterostructured nanocomposites with high activity in CO_2 photoreduction, Appl. Catal. B 231 (2018) 269–276, https://doi.org/10.1016/j.apcatb.2018.03.027.

[38] X.Y. Kong, W.L. Tan, B. Ng, S. Chai, Abdul Rahman Mohamed, Harnessing Vis-NIR broad spectrum for photocatalytic CO_2 reduction over carbon quantum dots-decorated ultrathin Bi_2WO_6 nanosheets, Nano Res. 10 (2017) 1720–1731, https://doi.org/10.1007/s12274-017-1435-4.

[39] J.X. Xia, J. Di, H.T. Li, H. Xu, H.M. Li, S.J. Guo, Ionic liquid-induced strategy for carbon quantum dots/BiOX(X = Br, Cl) hybrid nanosheets with superior visible-light-driven photocatalysis, Appl. Catal. B 181 (2016) 260–269, https://doi.org/10.1016/j.apcatb.2015.07.035.

[40] S.J. Zhu, Q.N. Meng, L. Wang, J.H. Zhang, Y.B. Song, H. Jin, K. Zhang, H.C. Sun, H.Y. Wang, B. Yang, Highly photoluminescent carbon sots for multicolor patterning, sensors, and bioimaging, Angew. Chem. Int. Ed. 52 (2013) 3953–3957, https://doi.org/10.1002/anie.201300519.

[41] Z.P. Chen, K.W. Mou, X.H. Wang, L.C. Liu, Nitrogen-Doped graphene quantum dots enhance the activity of Bi_2O_3 nanosheets for electrochemical reduction of CO_2 in a wide negative potential region, Angew. Chem. Int. Ed. 57 (2018) 12790–12794, https://doi.org/10.1002/anie.201807643.

[42] J. Di, J.X. Xia, M.X. Ji, L. Xu, S. Yin, Z.G. Chen, H.M. Li, Bidirectional acceleration of carrier separation spatially via N-CQDs/atomically-thin BiOl nanosheets nanojunctions for manipulating active species in a photocatalytic process, J. Mater. Chem. A 4 (2016) 5051–5061, https://doi.org/10.1039/c6ta00284f.

[43] R.L. Liu, D.Q. Wu, X.L. Feng, K. Müllen, Bottom-up fabrication of photoluminescent graphene quantum dots with uniform morphology, J. Am. Chem. Soc. 133 (2011) 15221–15223, https://doi.org/10.1021/ja204953k.

[44] J.M. Ma, X.D. Liu, J.B. Lian, X.C. Duan, W.J. Zheng, Ionothermal synthesis of BiOCl nanostructures via a long-chain ionic liquid precursor route, Cryst. Growth Des. 10 (2010) 2522–2527, https://doi.org/10.1021/cg100700f.

[45] Y.Z. Han, H. Huang, H.C. Zhang, Y. Liu, X. Han, R.H. Liu, H.T. Li, Z.H. Kang, Carbon quantum dots with photoenhanced hydrogen-bond catalytic activity in aldol

condensations, ACS Catal. 4 (2014) 781–787, https://doi.org/10.1021/cs401118x.
[46] L. Jiao, Y. Wang, H.L. Jiang, Q. Xu, Metal-organic frameworks as platforms for catalytic applications, Adv. Mater. 37 (2018) 1703663, , https://doi.org/10.1002/adma.201703663.
[47] Z. Zhang, J.T. Yates, Band bending in semiconductors: chemical and physical consequences at surfaces and interfaces, Chem. Rev. 112 (2012) 5520–5551, https://doi.org/10.1021/cr3000626.
[48] X.X. Chang, T. Wang, J.L. Gong, CO_2 photo-reduction: insights into CO_2 activation and reaction on surfaces of photocatalysts, Energy Environ. Sci. 9 (2016) 2177–2196, https://doi.org/10.1039/C6EE00383D.
[49] S.B. Wang, B.Y. Guan, X.W. Lou, Construction of $ZnIn_2S_4$-In_2O_3 hierarchical tubular heterostructures for efficient CO_2 photoreduction, J. Am. Chem. Soc. 140 (2018) 5037–5040, https://doi.org/10.1021/jacs.8b02200.
[50] J. Di, C. Zhu, M.X. Ji, M.L. Duan, R. Long, C. Yan, K.Z. Gu, J. Xiong, Y.B. She, J.X. Xia, H.M. Li, Z. Liu, Defect-rich $Bi_{12}O_{17}Cl_2$ nanotubes self-accelerating charge separation for boosting photocatalytic CO_2 reduction, Angew. Chem. Int. Ed. 45 (2018) 14847–14851, https://doi.org/10.1002/anie.201809492.
[51] J.N. Qin, S.B. Wang, H. Ren, Y.D. Hou, X.C. Wang, Photocatalytic reduction of CO_2 by graphitic carbon nitride polymers derived from urea and barbituric acid, Appl. Catal. B 179 (2015) 1–8, https://doi.org/10.1016/j.apcatb.2015.05.005.
[52] H. Wang, D.Y. Yong, S.C. Chen, S.L. Jiang, X.D. Zhang, W. Shao, Q. Zhang, W.S. Yan, B.C. Pan, Y.J. Xie, Oxygen-vacancy-mediated exciton dissociation in BiOBr for boosting charge-carrier-involved molecular oxygen activation, Am. Chem. Soc. 140 (2018) 1760–1766, https://doi.org/10.1021/jacs.7b10997.
[53] B. Wang, J. Di, G.P. Liu, S. Yin, J.X. Xia, Q. Zhang, H.M. Li, Novel mesoporous graphitic carbon nitride modified $PbBiO_2Br$ porous microspheres with enhanced photocatalytic performance, J. Colloid Interface Sci. 507 (2017) 310–322, https://doi.org/10.1016/j.jcis.2017.07.094.
[54] J. Li, X.Y. Wu, W.F. Pan, Ga.K. Zhang, H. Chen, Vacancy-rich monolayer BiO_{2-x} as a highly efficient uv, visible, and near-infrared responsive photocatalyst, Angew. Chem. Int. Ed. 56 (2017) 1–6, https://doi.org/10.1002/anie.201708709.
[55] S.B. Wang, B.Y. Guan, X.W. Lou, Rationally designed hierarchical N-doped carbon@$NiCo_2O_4$ double-shelled nanoboxes for enhanced visible light CO_2 reduction, Energy Environ. Sci. 11 (2018) 306–310, https://doi.org/10.1039/C7EE02934A.
[56] X.C. Jiao, Z.W. Chen, X.D. Li, Y.F. Sun, S. Gao, W.S. Yan, C.M. Wang, Q. Zhang, Y. Lin, Y. Luo, Y. Xie, Defect-mediated electron-hole separation in one-unit-cell $ZnIn_2S_4$ layers for boosted solar-driven CO_2 reduction, J. Am. Chem. Soc. 139 (2017) 7586–7594, https://doi.org/10.1021/jacs.7b02290.
[57] S. Gao, B.C. Gu, X.C. Jiao, Y.F. Sun, X.L. Zu, F. Yang, W.G. Zhu, C.M. Wang, Z.M. Feng, B.J. Ye, Yi Xie, Highly efficient and exceptionally durable CO_2 photoreduction to methanol over freestanding defective single-unit-cell bismuth vanadate layers, J. Am. Chem. Soc. 139 (2017) 3438–3445, https://doi.org/10.1021/jacs.6b11263.
[58] X.C. Jiao, X.D. Li, X.Y. Jin, Y.F. Sun, J.Q. Xu, L. Liang, H.X. Ju, J.F. Zhu, Y. Pan, W.S. Yan, Y. Lin, Y. Xie, Partially oxidized SnS_2 atomic layers achieving efficient visible-light-driven CO_2 reduction, J. Am. Chem. Soc. 139 (2017) 18044–18051, https://doi.org/10.1021/jacs.7b10287.
[59] P.F. Xia, B.C. Zhu, J.G. Yu, S.W. Cao, M. Jaroniec, Ultra-thin nanosheet assemblies of graphitic carbon nitride for enhanced photocatalytic CO_2 reduction, J. Mater. Chem. A 5 (2017) 3230–3238, https://doi.org/10.1039/C6TA08310B.
[60] W.K. Wang, D.F. Xu, B. Cheng, J.G. Yu, C.J. Jiang, Hybrid carbon@TiO_2 hollow spheres with enhanced photocatalytic CO_2 reduction activity, J. Mater. Chem. A 5 (2017) 5020–5029, https://doi.org/10.1039/C6TA11121A.
[61] Z.F. Jiang, H.L. Sun, T.Q. Wang, B. Wang, W. Wei, H.M. Li, S.Q. Yuan, T.C. An, H.J. Zhao, J.G. Yu, P.K. Wong, Nature-based catalyst for visible-light-driven photocatalytic CO_2 reduction, Energy Environ. Sci. 9 (2018) 2382–2389, https://doi.org/10.1039/C8EE01781F.
[62] J. Wu, X.D. Li, W. Shi, P.Q. Ling, Y.F. Sun, X.C. Jiao, S. Gao, L. Liang, J.Q. Xu, W.S. Yan, C.M. Wang, Y. Xie, Efficient visible-light-driven CO_2 reduction mediated by defect-engineered BiOBr atomic layers, Angew. Chem. Int. Ed. 57 (2018) 1–7, https://doi.org/10.1002/anie.201803514.